Article
Chinese Science Bulletin
Geophysics
July 2012 Vol.57 No.20: 2586–2594
doi: 10.1007/s11434-012-5130-2

Characteristics of tidal gravity changes in Lhasa, Tibet, China

XU JianQiao*, CHEN XiaoDong, ZHOU JiangCun & SUN HePing

State Key Laboratory of Geodesy and Earth's Dynamics, Institute of Geodesy and Geophysics, Chinese Academy of Sciences, Wuhan 430077, China

Received November 16, 2011; accepted February 17, 2012; published online April 24, 2012

Tidal gravity changes arise from the response of the solid Earth to the tidal forces of the Sun, Moon and planets close to the Earth, and are a comprehensive reflection of the structure and distribution of physical properties of the Earth's interior. As a result, observations of tidal gravity changes are the basis of studies on other global and/or regional dynamic processes. The characteristics of tidal gravity changes in the region of the Tibetan Plateau were investigated through continuous gravity measurements recorded with a superconducting gravimeter (SG) installed in Lhasa over a year. Through contrast measurements with a spring gravimeter LaCoste-Romberg ET20 at the same site, the gravity observations in Lhasa were scaled to the international tidal gravity reference in Wuhan. Meanwhile, the scale factor of the SG was determined accurately as -777.358 ± 0.136 nm s^{-2} V^{-1}, which is about 2.2% less than the value provided by the manufacturer. The results indicate that the precision of the tidal gravity observations made with the SG in Lhasa was very high. The standard deviation was 0.459 nm s^{-2}, and the uncertainties of for the four main tidal waves (i.e. O_1, K_1, M_2 and S_2) were better than 0.006%. In addition, the observations of the diurnal gravity tides had an obvious pattern of nearly diurnal resonance. As a result, it is affirmed that the Lhasa station can provide a local tidal gravity reference for gravity measurements on the Tibetan Plateau and its surrounding regions. The loading effects of oceanic tides on tidal gravity observations in Lhasa are so weak that the resulting perturbations in the gravimetric factors are less than 0.6%. However, the loading effects of the local atmosphere on either the tidal or nontidal gravity observations are significant, although no seasonal variations were found. After removal of the atmospheric effects, the standard deviation of the SG observations in Lhasa decreased obviously from 2.009 to 0.459 nm s^{-2}. Having removed the loading effects of oceanic tides and local atmosphere, it was found that the tidal gravity observations made with the SG in Lhasa significantly differed by about 1% from those expected theoretically, which may be related to active tectonic movement and the extremely thick crust in the region of the Tibetan Plateau. A more-certain conclusion requires longer accumulation of SG data and further associated theoretical studies.

Tibetan Plateau, Lhasa, gravimetric parameters, superconducting gravimeter, nearly diurnal resonance, loading effects

Citation: Xu J Q, Chen X D, Zhou J C, et al. Characteristics of tidal gravity changes in Lhasa, Tibet, China. Chin Sci Bull, 2012, 57: 2586–2594, doi: 10.1007/s11434-012-5130-2

The dominant component of the attractive forces of the Sun, Moon and nearby planets acting on the Earth maintains the Earth's orbit in space, and the small remainder (i.e. tide-generating forces) leads to the periodic tidal deformation of the solid Earth and tidal variations in the Earth's gravity field. The changes in tidal gravity are the response of the solid Earth to the tide-generating forces, and are a comprehensive reflection of the structure and distribution of physical properties in the Earth's interior. They are the dominant part of temporal gravity changes and have a very high signal-to-noise ratio in gravity measurements. On the one hand, the tide-generating forces or potential at any site on the Earth can be deduced accurately using Newton's law of universal gravitation and precise orbit parameters of the related celestial bodies obtained from the modern astronomic measurements [1–6]. Based on available equilibrium Earth models, the Earth's tidal deformation, including tidal gravity variations, can be determined theoretically through

*Corresponding author (email: xujq@asch.whigg.ac.cn)

numerical integration of the tidal movement equations; i.e. the coupled elastic movement equations, mass conservation equations, constitutive equations and Poisson's equation [7–10]. The Earth's tidal deformation is a geophysical phenomenon that can be predicted accurately. On the other hand, tidal gravity variations can also be determined through long-term continuous observations with a high-precision gravimeter installed on the Earth's surface. The gravimetric parameters can be evaluated accurately in different tidal frequency bands through harmonic analysis [11–14]. Observations and theoretical investigation of tidal gravity changes provide important information for determining the structure of the Earth's interior, and they are the basis of studies on other global and local geodynamic processes.

The Tibetan Plateau is located in the convergent region of the Pacific Plate, Indian Plate and Eurasian Plate. The plateau is the youngest orogen, and it is the largest and highest plateau in the world. It is referred to as the Earth's third pole. Since the early 20th century, many geodetic strategies, including trigonometric surveys, arc measurements, leveling surveys, Global Positioning System measurements, and gravity measurements, have been carried out by many international research institutes to determine the present-day crustal deformation and movement of the Tibetan Plateau. The geodetic measurements have provided abundant information and basic data for studies on the mechanism of the tectonic movements of the plateau and led to some significant results [15]. In China, although some progresses have been made in the observations and investigations of gravity tides on the Tibetan Plateau [16], the primary results are not conclusive owing to their poor precision, the instability of the used instruments and the short measurement period of half a year. The thickness of the crust in the region of the Tibetan Plateau is 65 to 75 km [15], which is at least approximately 3 times the mean value for the whole Earth. It needs to be clarified whether the Earth's response to tidal forces in the Tibetan region is strongly affected by active tectonic movement and the extremely thick crust of the plateau, and whether the loading effects have any special pattern in this area.

The superconducting gravimeter (SG) is the best instrument for gravity measurements owing to its advantages of very high sensitivity and stability, extremely low noise level and drift, and wide frequency range of the dynamic response. SG precision can reach the order of 10^{-2} nm s^{-2}. As a result, the SG plays an important role in studies on global and regional geodynamics, especially those on the vertical crust movement [17–21]. Lhasa is located in the southern part of the Tibetan Plateau, on the northern side of the Himalayan Mountains and on flat land in a valley in the middle reaches of the Lhasa River, which is a tributary of the Brahmaputra. A permanent station of continuous gravity measurements was set up in Lhasa by the Institute of Geodesy and Geophysics, Chinese Academy of Sciences, at the end of 2009 to investigate hotspots of geodynamical research such as the formation, evolution, uplifting rate, and related dynamical mechanisms of the Tibetan Plateau. An SG was installed at the Lhasa station to monitor continuous long-term local gravity variations. The main motivation of the present study is to investigate the nature of tidal gravity changes and the loading effects on the Tibetan plateau, to determine accurately the gravimetric parameters, and to establish regional preparatory references for gravity tides.

1 Calibration of the SG in Lhasa

A permanent gravity station was set up in Lhasa on the southern Tibetan Plateau by the Institute of Geodesy and Geophysics, Chinese Academy of Sciences, at the end of 2009. The geographical coordinates of the station are 29.645°N, 91.035°E, and the altitude of the station is 3632.3 m. The station comprises an SG measurement room, an SG monitoring room and a room for contrast gravity measurements. Two square observation piers with side lengths of 1.2 m were built in the contrast measurement room for convenient contrast observations of a relative or absolute gravimeter with the SG. An SG (denoted C057) was installed on an equilateral-triangle pier with side lengths of 77 cm. All the observation piers, which are 1 m in height, were concreted together with a 30-cm-thick bedding base, and separated from the surroundings by 10 cm to avoid perturbation from environmental noise. A computer in the monitoring room controls the SG and its accessories by setting associated parameters via a control system. Meanwhile, the working status of the instrument can be monitored through the real-time display of pictures and related parameters. The data, including the gravity, barometric pressure, and temperature data, are recorded automatically and stored by the computer. In addition, the control system allows remote monitoring, control and data transference via the Internet.

Being similar to a spring gravimeter, the SG is a relative gravimeter, and its output is a voltage describing relative gravity changes. Although the primary scale factor (i.e. the transfer function from the output voltage to the relative gravity change) is provided by the manufacturer, the value is not accurate enough to satisfy the requirement of high-precision gravity observations. Therefore, the scale factor of the SG must be calibrated accurately.

Through extensive international cooperation and continuous long-term comparative observations with several high-precision gravimeters, especially continuous long-term observations with an SG at the Wuhan station, an international tidal gravity reference in Wuhan has been established [22]; the gravimetric parameters, including the amplitude factor δ and phase difference $\Delta\varphi$, of the main tidal waves O_1, K_1, M_2 and S_2 in Wuhan were determined accurately. A high-precision spring gravimeter, LaCoste-Romberg (LCR) ET20, has operated at the Wuhan station for a long period.

The standard deviation of the tidal gravity observations was 7.455 nm s^{-2}, and the precision for the main tidal waves was better than 0.16%. Owing to strong contamination of local barometric pressure in the observations of tidal wave S_2, as well as significant temperature disturbance near the frequency of wave S_2, the amplitude factor determined from LCR-ET20 measurements significantly differed from the value determined from the tidal gravity reference in Wuhan. The amplitude factors of tidal waves O_1, K_1 and M_2 were accurately determined as 1.17655, 1.14725 and 1.17281, differing respectively by 0.12%, 0.43% and 0.15% from the corresponding values obtained from the tidal gravity reference in Wuhan. This implies that the scale factor of LCR-ET20 has been normalized to the international tidal gravity reference in Wuhan, and a relative gravimeter can be calibrated accurately through measurements parallel to LCR-ET20.

To determine accurately the SG scale factor at the Lhasa station, and to normalize the tidal gravity observations in Lhasa to the international tidal gravity reference in Wuhan, LCR-ET20 was installed simultaneously in the contrast gravity measurement room of the Lhasa station to carry out parallel observations with the SG. Figure 1 illustrates the contrast in gravity observations made by LCR-ET20 and SG-C057 at the Lhasa station from December 8 to 12, 2009. It is found that the measurements made by these two instruments had similar patterns except that there were very tiny drifts in the gravity observations, $\Delta g(t)$, made with LCR-ET20. After primary preprocessing and harmonic analysis of the data recorded simultaneously with SG-C057 and LCR-ET20 at the Lhasa station from December 8, 2009 to February 27, 2011, the gravimetric amplitude factors of the main tidal waves were estimated. The analysis indicates that although the standard deviation of LCR-ET20 measurements was as large as 11.720 nm s^{-2}, the precision of the amplitude-factor estimations of the main tidal waves was better than 0.2%; the standard deviation of SG-C057 measurements was 2.009 nm s^{-2} and the precision of the amplitude factor estimations of the main tidal waves was better than 0.05%. Because the observations of tidal wave S_2 were heavily contaminated by local barometric pressure, the weighted average of the amplitude (or amplitude factor) ratios of tidal waves O_1, K_1 and M_2 observed with LCR-ET20 to those observed with SG-C057 was used to scale the measurements made by SG-C057, where the reciprocal of the standard deviation of each tidal wave observed with SG-C057 was chosen as the corresponding weight function. As a result, the scale factor of SG-C057 at the Lhasa station was accurately determined as –777.358 ± 0.136 nm s^{-2} V^{-1}, which is about 2.2% less than the value provided by the manufacturer (i.e. –795 nm s^{-2} V^{-1}). The relative precision of calibration was as high as 0.02%, which satisfied completely the requirements of high-precision continuous gravity measurements.

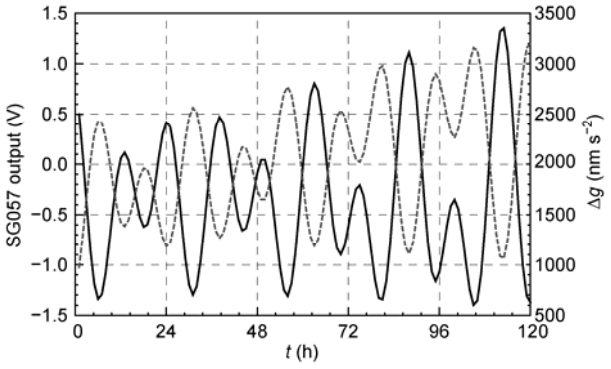

Figure 1 Comparison between observations with the SG (solid line) and observations with LCR-ET20 (dashed line) at the Lhasa station from December 8 to 12, 2009.

2 Analysis of the observations

The SG at the Lhasa station began normal recording of the temporal gravity variations on December 8, 2009. Related data, including gravity, barometric pressure and temperature data, have been continuously and automatically acquired and stored by the computer with a sampling rate of 1 s. The continuous gravity change $\Delta g(t)$ of 447 d duration, depicted in Figure 2, are available and have the potential to describe the pattern of local tidal gravity variations.

The software package T-Soft [23], which is recommended by the International Center of the Earth's Tides for the analysis of Earth tide data, was employed to preprocess the gravity data recorded with the SG at the Lhasa station. Using interactive removal-restoring technology, some incorrect records, such as spikes, steps, offsets and vibrations due to strong earthquakes, were graphically removed and then corrected. Some short gaps due to chance events, such as sudden interruption of the electricity supply and instrument failure, were interpolated using polynomials or spline functions. Additionally, 1-s-sampled data series were transformed to 1-h-sampled data series using a low-pass digital filter. Eterna3.30, a standard harmonic analysis software package [24], was used to analyze the tidal gravity observations recorded with the SG at the Lhasa station. The gravimetric parameters were thus accurately determined and are

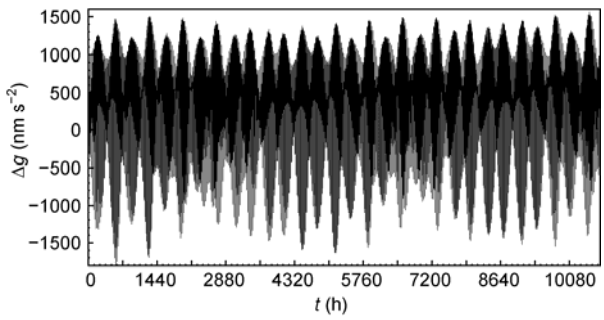

Figure 2 Tidal gravity changes observed with the SG at the Lhasa station from December 8, 2009 to February 27, 2011.

tabulated in Table 1. In harmonic analysis, a high-precision tidal generating potential, developed by Hartmann and Wenzel, was used. The analysis results indicate that the precision of tidal gravity observations made with SG-C057 at the Lhasa station was very high. The standard deviation was as little as 0.459 nm s^{-2}, the gravimetric parameters (δ, $\Delta\varphi$) of the four main tidal waves were accurately estimated as (1.17031±0.00006, –0.0148°±0.0030°) for O_1, (1.14430 ± 0.00006, 0.0656°±0.0028°) for K_1, (1.17205±0.00002, –0.4619°±0.0012°) for M_2 and (1.16609±0.00006, –0.6719° ±0.0043°) for S_2, where the estimation precision of the amplitude factors is better than 0.006%. The estimation precision for all other tidal waves with amplitudes exceeding 20 nm s^{-2} was better than 0.09%. This implies that the tidal gravity observations made with SG-C057 at the Lhasa station can be regarded as a regional tidal gravity reference for gravity measurements on the Tibetan Plateau and its surrounding regions.

The Earth's tidal deformation, including tidal gravity changes, is a geodynamical phenomenon that can be

Table 1 Tidal gravity observations recorded with the SG at the Lhasa station

Waves	Frequency range (cpd)	Theoretical amplitude (nm s^{-2})	Observations with SG-C057[a]				After oceanic tides correction		Theoretical model δ [8]
			δ	$\sigma(\delta)$	$\Delta\varphi$ (°/h)	$\sigma(\Delta\varphi)$ (°)	δ	$\Delta\varphi$ (°)	
SGQ_1	0.721499–0.833113	1.9721	1.15632	0.00672	0.4489	0.3333	1.13735	–0.8822	1.1560
$2Q_1$	0.851181–0.859691	6.7640	1.17095	0.00216	0.6303	0.1058	1.15740	–0.1513	1.1559
σ_1	0.860895–0.870024	8.1634	1.17487	0.00185	0.3915	0.0901	1.16218	–0.3193	1.1559
Q_1	0.887326–0.896130	51.1178	1.17354	0.00030	0.2419	0.0147	1.16601	–0.0982	1.1558
ρ_1	0.897806–0.906316	9.7096	1.17605	0.00166	0.2439	0.0806	1.16862	–0.0545	1.1558
O_1	0.921940–0.930450	266.9857	1.17031	0.00006	–0.0148	0.0030	1.16601	–0.1473	1.1556
τ_1	0.931963–0.940488	3.4822	1.15969	0.00523	0.3651	0.2585	1.15655	0.3035	1.1556
NO_1	0.958085–0.966757	20.9974	1.16565	0.00061	–0.1157	0.0299	1.16430	–0.0249	1.1550
χ_1	0.968564–0.974189	4.0158	1.15742	0.00424	–0.3590	0.2097	1.15745	–0.3652	1.1549
π_1	0.989048–0.995144	7.2651	1.15064	0.00274	–0.9963	0.1358	1.15216	–1.0593	1.1517
P_1	0.996967–0.998029	124.2278	1.15848	0.00017	–0.0164	0.0085	1.16042	–0.0835	1.1501
S_1	0.999852–1.000148	2.9377	1.59122	0.01868	19.2170	0.6467	1.59231	19.1359	1.1467
K_1	1.001824–1.003652	375.4852	1.14430	0.00006	0.0656	0.0028	1.14728	–0.0989	1.1346
Ψ_1	1.005328–1.005624	2.9377	1.25380	0.00711	0.0489	0.3239	1.25537	–0.0335	1.2403
Φ_1	1.007594–1.013690	5.3469	1.17415	0.00366	–0.2682	0.1790	1.17622	–0.3916	1.1705
θ_1	1.028549–1.034468	4.0151	1.16968	0.00408	–0.2458	0.1995	1.17269	–0.5676	1.1579
J_1	1.036291–1.044801	20.9966	1.16516	0.00079	0.0358	0.0387	1.16857	–0.3653	1.1576
SO_1	1.064840–1.071084	3.4829	1.17457	0.00465	–0.3712	0.2268	1.17807	–1.1172	1.1570
OO_1	1.072582–1.080945	11.4890	1.16380	0.00110	–0.0100	0.0540	1.16672	–0.8196	1.1569
ν_1	1.099160–1.216398	2.1997	1.16226	0.00543	–0.2154	0.2675	1.16507	–1.6772	1.1567
ε_2	1.719380–1.837970	4.1907	1.18286	0.00292	–0.3033	0.1415	1.18313	0.4930	1.1594
$2N_2$	1.853919–1.862429	14.3723	1.17902	0.00092	–0.5942	0.0449	1.17807	0.0564	1.1594
μ_2	1.863633–1.872143	17.3450	1.17859	0.00081	–0.5226	0.0393	1.17695	0.1048	1.1594
N_2	1.888386–1.896749	108.6131	1.17412	0.00013	–0.5746	0.0061	1.17267	–0.0861	1.1594
ν_2	1.897953–1.906463	20.6300	1.17257	0.00069	–0.6038	0.0336	1.17067	–0.1272	1.1594
M_2	1.923765–1.942754	567.2884	1.17205	0.00002	–0.4619	0.0012	1.17158	–0.1074	1.1594
λ_2	1.958232–1.963709	4.1832	1.16930	0.00335	–0.5914	0.1643	1.16971	–0.3359	1.1594
L_2	1.965826–1.976927	16.0345	1.17619	0.00121	–0.4323	0.0592	1.17629	–0.1862	1.1594
T_2	1.991786–1.998288	15.4312	1.17115	0.00095	–0.8619	0.0466	1.17334	–0.6894	1.1594
S_2	1.999705–2.000767	263.9324	1.16609	0.00006	–0.6719	0.0043	1.17016	–0.5182	1.1594
K_2	2.002590–2.013690	71.7503	1.16725	0.00018	–0.3915	0.0087	1.17086	–0.2621	1.1594
η_2	2.031287–2.047391	4.0117	1.16654	0.00278	–0.0783	0.1363	1.17422	–0.0194	1.1594
$2K_2$	2.067578–2.182844	1.0507	1.16610	0.00731	0.0214	0.3592	1.17904	0.0165	1.1594
MN_3	2.753243–2.869714	2.6583	1.08240	0.00298	–0.0501	0.1579	1.08240	–0.0501	1.0718
M_3	2.892639–3.081255	9.6883	1.08231	0.00085	0.0179	0.0451	1.08231	0.0179	1.0718
M_4	3.791963–3.937898	0.1533	1.00029	0.03545	–1.1772	2.0306	1.03340	0.5966	1.0359

a) $\sigma(\delta)$ and $\sigma(\Delta\varphi)$ are the standard deviations of the amplitude factor δ and phase difference $\Delta\varphi$, respectively.

described accurately through theoretical simulation. Using a rotating, elliptical and non-hydrostatic equilibrium Earth, the Earth's tidal movements were simulated theoretically by Dehant et al. [8] in 1999 through displacement truncation, where the anelasticity of the media in the mantle, mantle convection and excited deformation of the mantle boundaries were considered. The gravimetric parameters and Love numbers in various tidal frequency bands were determined. As a result, an accurate theoretical model of the Earth's tides was developed (denoted DDW99). For convenience of comparison, the gravimetric amplitude factors expected theoretically in DDW99 are also tabulated in Table 1. Comparing the gravimetric amplitude factors retrieved from the SG-C057 measurements at the Lhasa station with those expected in DDW99, it is found that their differences were very small, their standard deviation was only 0.00987, and the differences for the several tidal waves with largest amplitudes, namely O_1, P_1, K_1, N_2, M_2, and S_2, were about 1%. This means that the loading effects of oceanic tides on the tidal gravity observations are very weak in the Lhasa region owing to the station being far from the ocean.

3 Loading effects of oceanic tides and atmosphere

The dominant component of the observed residuals of the gravity tides is mainly due to the loading effects of global and local oceanic tides, including direct effects (i.e. Newton's attraction due to the mass of ocean water) and indirect effects (i.e. deformation of the Earth's surface and additional gravitational potential due to mass redistribution in the Earth's interior). In the most areas of the world, the loading effects of oceanic tides can reach 1%–2% of the magnitude of gravity tides. Furthermore, they can be as large as 3%–4% of the magnitude of gravity tides in coastal regions. According to the classical theory of surface loads, the loading effects of the oceanic tides, including amplitude L and phase λ, can be simulated by means of global convolution integration of the height of each oceanic tide and Green's functions of surface loads [25–27]. In 1980, Schwiderski developed the first available global model of oceanic tides [28]. With the development of satellite altimeters and the long-term accumulation of their data, more and more global models of oceanic tides with higher precision and higher spatial resolution have been developed [29–33].

The global oceanic tides model Nao99 [32] with spatial resolution of 0.5° × 0.5°, developed by Matsumoto et al through the assimilation of 5-year data recorded by the Topex/Poseidon altimeter and the data recorded by many tide gauges around Japan, was used in this study. Compared with other global oceanic tides models, the regional ocean tides in the shallow area around Japan were significantly improved in Nao99, and the model is thus the most appropriate for loading correction of oceanic tides in the Asian area. Nao99 provides digital co-tidal maps of seven diurnal tidal waves (i.e. Q_1, O_1, M_1, P_1, K_1, J_1 and OO_1) and eight semidiurnal tidal waves (i.e. μ_2, N_2, ν_2, M_2, L_2, T_2, S_2 and K_2) with relatively large amplitudes. The loading vector $\boldsymbol{L}(L, \lambda)$ of each of these tidal waves was obtained using the algorithm of integrated Green's functions [27] and is presented in Table 2. The numerical results indicate that the tidal gravity observations recorded at the Lhasa station were only slightly affected by the oceanic tide loading because Lhasa is located on an inland plateau far from the ocean. In consideration of the magnitude of each tidal wave at the Lhasa station, the loading effects of oceanic tides on the tidal gravity observations in the semidiurnal frequency band are slightly stronger. Among these tidal waves, M_2 has the largest amplitude for the loading vector of oceanic tides of 4.122 nm s^{-2}, which is only about 0.6% of the observed amplitude for gravity tides. In the diurnal frequency band, the strongest effect of oceanic tide loads on gravity tides is that for K_1, whose amplitude is only 1.667 nm s^{-2}, or about 0.4% of the observed amplitude.

For the other tidal waves with lower amplitudes, the oceanic tide loading vectors were obtained by interpolating or extrapolating in the frequency domain [34]. The loading vector of the oceanic tide for wave M_4 was obtained using the co-tide maps provided by global oceanic tides model Fes2004.

Using the phasor difference of the observed vector of gravity tides and the loading vector of oceanic tides for each wave, the loading effects of oceanic tides were removed from the tidal gravity observations, and the gravimetric parameters after correction of the oceanic tide loading were obtained and tabulated also in Table 1. The numerical results indicate that the oceanic tide loads induced very little perturbation in the gravimetric parameters recorded at the Lhasa station, and the perturbation in the gravimetric parameters excited by the oceanic tide loads were less than 0.6% for the tidal waves with amplitude exceeding 20 nm s^{-2}.

Table 2 Vector of the gravity changes induced by loading effects of the oceanic tides at the Lhasa station[a)]

	Q_1	O_1	M_1	P_1	K_1	J_1	OO_1	μ_2	N_2	ν_2	M_2	L_2	T_2	S_2	K_2
L(nms^{-2})	0.524	1.356	0.048	0.294	1.667	0.186	0.192	0.226	1.098	0.205	4.122	0.081	0.064	1.355	0.321
λ (°)	42.75	32.07	−54.01	144.95	132.16	112.53	99.65	−82.94	−82.10	−79.31	−86.55	−91.41	−122.65	−142.97	−144.18

a) Loading vectors of tidal waves O_1, K_1, M_2 and S_2 with the largest amplitudes were simulated by combining the global oceanic tide model and the local co-tides for China; those of the other tidal waves were computed using Nao99 only.

Having removed the loading effects of oceanic tides, the amplitude factors of gravity tides, measured with the SG at the Lhasa station, only changed slightly, with the amplitude factors decreasing respectively 0.6%, 0.4% and 0.1% for Q_1, O_1 and N_2, while they increased 0.2%, 0.3%, 0.3% and 0.3% for tidal waves P_1, K_1, S_2 and K_2, respectively, and the amplitude factor of M_2 hardly changed. On the whole, the observations were closer to the theoretical and experimental models for the gravity tides after correction, and the standard deviation between the SG057 observations in Lhasa and theoretical model DDW99 decreased from 0.00987 to 0.00771.

The loading effects of barometric pressure are the largest noise source in the tidal gravity observations except for the oceanic tide loads. As a result, the atmospheric effects should be effectively removed from the measurements of gravity tides. Previous studies indicated that the loading effects of barometric pressure on gravity observations predominantly arise from the contribution of the local atmosphere surrounding the station, and the effects mainly concentrated on the annual and seasonal variations in the long-period frequency band and the vibrations of the atmospheric tides from S_1 to S_{12} with periods from 1 to 12 cycles per day, which relate to solar heating. The atmosphere within 50 km of the station accounted for 90%–95% of the atmospheric influence [35–39], which has been confirmed by the measurements with the SGs at globally distributed stations. The loading effects of local atmosphere can be described as a transfer function from the station barometric pressure to nontidal gravity variations, which is called atmospheric gravity admittance because of strong correlation between the variations in the atmospheric pressure at the station and those in the local area surrounding the station. Continuous gravity observations made with the SGs distributed globally indicate that the atmospheric effects evaluated using the station barometric pressure were in good agreement with those simulated using either local or global barometric pressure. The atmospheric gravity admittance was about -3.360 nm s^{-2} hPa^{-1}, depending on the location of the station and frequencies of the signatures [14,39,40]. The measurement results indicate that there were no obvious seasonal or annual variations in the local atmospheric pressure at the Lhasa station, unlike the case in areas of low or moderate latitude. The pressure changes were mainly concentrated on the short-period perturbations and their magnitudes reached as high as −30 hPa. In the period from June to September, the predominant components of the local barometric pressure variations were high-frequency vibrations with smaller magnitudes, while the frequencies of the barometric pressure variations and the magnitudes increased in the remaining period. The atmospheric gravity admittance was estimated as -3.740 ± 0.006 nm s^{-2} hPa^{-1} at the Lhasa station, and did not significantly differ from values either predicted by theoretical simulation or obtained with the SGs at stations in other areas [14, 35–40]. To show intuitively the loading effects of local barometric pressure on the gravity measurement, Figure 3 depicts the nontidal gravity variations measured with the SG and those induced by local barometric pressure at the Lhasa station. It is found that almost all the obvious gravity disturbances were related to the loading effects of local atmospheric pressure. The magnitudes of pressure-induced gravity changes reached as high as 112.3 nm s^{-2}. The pressure considerably affected the gravity measurements in each frequency band. The harmonic analysis results indicate that when the atmospheric effects were removed, the standard deviation of the tidal gravity observations made with the SG at the Lhasa station significantly decreased from 2.009 to 0.459 nm s^{-2}, the noise levels decreased from 0.1385, 0.0576, 0.0366 and 0.0237 nm s^{-2} to 0.0210, 0.0170, 0.0105 and 0.0074 nm s^{-2} in diurnal, semidiurnal, terdiurnal and quarter-diurnal frequency bands, respectively, and the white-noise level decreased from 0.0364 to 0.0079 nm s^{-2}.

4 Discussion and conclusion

The Wuhan station is unique fundamental one for the international tidal gravity reference in the Asian continent. Through long-term contrast measurements with a high-precision spring gravimeter, LCR-ET20, at the Wuhan and Lhasa stations, the SG installed at the Lhasa station can be calibrated accurately. Meanwhile, the tidal gravity observations at the Lhasa station can be normalized to the international tidal gravity reference. Matching the tidal gravity observations of the several largest-amplitude waves (including O_1, K_1 and M_2) with LCR-ET20 and SG057 data, the scale factor of SG057 installed at the Lhasa station was determined accurately as -777.358 ± 0.136 nm s^{-2} V^{-1}, which is about 2.2% less than the value provided by the manufacturer (i.e. -795 nm s^{-2} V^{-1}). The calibration precision was 0.02% and satisfied the requirement of high-precision continuous gravity measurements.

The loading effects of oceanic tides and local barometric pressure on the tidal gravity observations made at the Lhasa station were investigated. Applying the classical theory of surface loads, the loading effects of oceanic tides on the

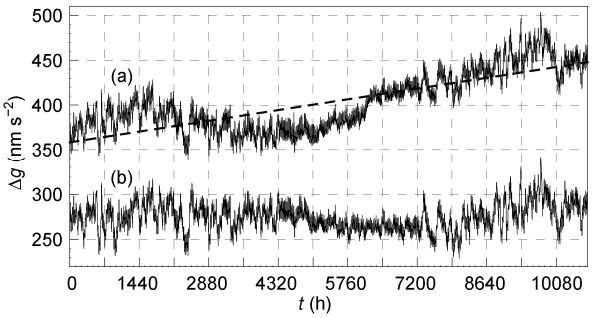

Figure 3 Comparison of the gravity residuals (a) and gravity changes induced by local barometric pressure (b).

tidal gravity observations made at the Lhasa station were theoretically computed using the global oceanic tide model Nao99 and the numerical method of integrated Green's functions. The numerical results indicate that the oceanic tide loads only induced tiny gravity changes at the Lhasa station, whose magnitudes were less than 0.6% of the observed amplitude of each tidal wave. The loading effects of oceanic tides on the gravimetric parameters were also very tiny. To validate the oceanic tide model used in this study, several numerical experiments had been made using the oceanic tide models of Schwiderski, Got00, Fes04 and Tpxo07; all the results were very close to those obtained using oceanic tide model Nao99. The noise in the tidal gravity observations made with the SG at the Lhasa station mainly arose from the loading effects of local atmospheric pressure. The local pressure changes were mainly short-period perturbations and there were no obvious seasonal variations in the region. The atmospheric gravity admittance was evaluated as -3.740 ± 0.006 nm s^{-2} hPa^{-1} at the Lhasa station and was in agreement with values predicted theoretically and observed in other areas. The pressure-induced gravity variations were great in each frequency band and the largest magnitude reached 112.3 nm s^{-2}. Having removed the loading effects of local pressure, the nontidal gravity disturbance observed with SG057 became much quieter and the standard deviation significantly decreased from 2.009 to 0.459 nm s^{-2}. With complete startup of the monitoring network of the tectonic environment of the Chinese continent, many absolute and relative gravity measurements have been carried out on the Tibetan Plateau and its surrounding regions. Because of their particularity, the loading effects of local barometric pressure should be carefully taken into account to obtain high-precision gravity data to meet the requirements of dynamic research in the related regions.

After careful preprocessing, treatment and analysis of the tidal gravity measurements recorded with SG057 from December 8, 2009 to February 27, 2011 at the Lhasa station, and after removal of the loading effects of local atmospheric pressure, the gravimetric parameters were determined accurately. The results indicate that the precision of the tidal gravity observations with SG057 in Lhasa was very high, and the standard deviation was 0.459 nm s^{-2}. The precision of the estimation of gravimetric parameters of the four main tidal waves O_1, K_1, M_2 and S_2 was better than 0.006% while that of the other tidal waves with amplitude exceeding 20 nm s^{-2} was better than 0.09%. Therefore, the tidal gravity observations made with SG057 at the Lhasa station can be regarded as a regional tidal gravity reference for the gravity measurements and dynamic research on the Tibetan Plateau and its surrounding regions, especially for the establishment of a monitoring network for the tectonic environment of the Chinese continent.

The tidal gravity observations made with SG057 at the Lhasa station have the potential to obtain information on some unknown features of the Earth's tidal deformation because of their extremely high precision. Having removed the loading effects of oceanic tides and local barometric pressure, it is found that the tidal gravity observations significantly differed from the values recently expected theoretically, with the difference for the four main tidal waves ranging from 0.9% to 1.4% and averaging about 1%; the detailed numerical results are presented in Table 1. The results of theoretical simulation and actual measurements of the gravity tides indicate that the tidal gravity variations are actually global long-wavelength signatures describing the response of an average Earth to the tide-generating forces imparted by celestial bodies [10]. The Earth's rotation, ellipticity and inelasticity only lead to tiny disturbances of Love numbers and gravimetric amplitude factors of the body tides. Their greatest contribution is the resonant enhancement of the Love numbers and the gravimetric amplitude factors of the diurnal tides related to their frequencies. The difference between the gravimetric amplitude factors of the main tidal waves observed and those expected theoretically should be no more than about 0.4% in most areas in the world [11–14,16,22]. It is affirmed that the relatively large difference between the gravimetric amplitude factors observed with SG057 at the Lhasa station and those expected theoretically is associated with the regional structure anomalies relative to the mean Earth model or other local perturbation elements except atmospheric pressure and oceanic tides. As is well known, in the area of the Tibetan Plateau, the largest local perturbation is due to variations in the glaciers covering the plateau. However, glacier ablation and its associated rebound are long-term slow processes and hardly affect the tidal deformation of the Earth. As a result, it is acceptable that the relatively large difference between the gravimetric amplitude factors observed with SG057 at the Lhasa station and those expected theoretically might be due to the combined contribution of the active tectonic movement of the Tibetan Plateau and its surrounding areas and the regional extremely thick crust. Of course, a more certain conclusion cannot be drawn until SG data are accumulated for a longer period and further associated theoretical studies are carried out.

Because of the interaction between the elliptical fluid core and the solid deformable mantle, the core has a nearly diurnal free wobble (NDFW) relative to the whole Earth, and behaves as a free core nutation (FCN) in the inertial space, which leads to resonant enhancement in the observations of the diurnal gravity tides and gravimetric amplitude factors of the diurnal tidal waves depending on their frequencies. These are important characteristics of the tidal gravity observations [7–10,14,41]. Using tidal gravity observations with SG057 at the Lhasa station, the nearly diurnal resonance parameters were fitted, and the FCN period was retrieved as 450.5 ± 8.6 sidereal days, which is slightly longer than those retrieved by stacking the tidal gravity observations made with global SGs [14,41]. The main reason is the tiny departure of the gravimetric parameters observed

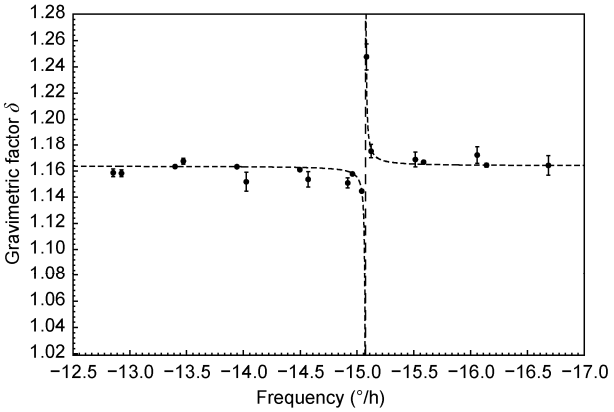

Figure 4 Nearly diurnal resonance observed with the SG at the Lhasa station. The dots with error bars stand for the gravimetric amplitude factors observed with the SG, the dashed hyperbolic curves depict the nearly diurnal resonance curves and the dashed vertical line indicates the frequency of the NDFW retrieved from the SG observations.

with the SG at the Lhasa station due to the active tectonic movement of the Tibetan Plateau and its surrounding areas and the regional extremely thick crust. Even so, the gravimetric amplitude factors observed with the SG at the Lhasa station clearly had a pattern of nearly diurnal resonance, which is depicted in Figure 4.

On all accounts, the tidal gravity observations made with the SG at the Lhasa station clearly indicate that the tidal gravity changes and loading effects of oceanic tides and local barometric pressure behave obviously the regional particularities, and the observations provide reliable references and correction models for related measurements and studies in this area, especially for the building of a monitoring network of the tectonic environment on the Chinese continent and subsequent research. With the accumulation of SG data at the Lhasa station, the long-term gravity changes related to the tectonic movement of the plateau will be obtained and provide a constraint for studies on regional continental dynamics.

The authors thank the staff at the Wuhan and Lhasa stations for providing high-quality SG data and Wang Chenchen for her careful preprocessing and analysis of the SG data. This work was supported by the National Natural Science Foundation of China (40874038, 41074053 and 41021003).

1 Doodson A T. The harmonic development of the tide generating potential. Proc Roy Soc Lond Ser A, 1954, 31: 37–61
2 Cartwright D E, Tayler R J. New computations of the tide generating potential. Geophys J R Astro Soc, 1971, 23: 45–74
3 Xi Q W. The algebraic deduction of the harmonic development for the tide generating potential with the IBMPC. In: Proceedings of the 10th international symposium on the Earth tides, Madrid, 1985. 481–489
4 Tamura Y. A harmonic development of the tidal generating potential. Bull Inf Marées Terres, 1987, 99: 6813–6815
5 Hartmann T, Wenzel H G. the HW95 tidal generating potential catalogue. Geophys Res Lett, 1995, 22: 3553–3556
6 Roosbeek F A. A harmonic development of the tide generating potential. Geophys J Int, 1996, 126: 197–204
7 Wahr J M. Body tides on an elliptical, rotating, elastic and oceanless earth. Geophys J R Astr Soc, 1981, 64: 677–703
8 Dehant V, Defraigne P, Wahr J. Tides for a convective Earth. J Geophys Res, 1999, 104: 1035–1058
9 Mathews P M. Love numbers and gravimetric factor for diurnal tides. J Geod Soc Jpn, 2001, 46: 231–236
10 Xu J Q, Sun H P. Deformation response of a SNREI Earth to surface loads and tidal forces (in Chinese). Chin J Geophys, 2003, 46: 328–343
11 Melchior P. A new data bank for tidal gravity measurements (DB92). Phys Earth Planet Inter, 1994, 82: 125–155
12 Melchior P, Ducarme B, Francis O. The response of the Earth to tidal body forces described by second- and third-degree spherical harmonics as derived from a 12 year series of measurement with the superconducting gravimeter GWR/T3 in Brussels. Phys Earth Planet Inter, 1996, 93: 223–238
13 Ducarme B, Venedikov A, Arnosob J, et al. Determination of the long period tidal waves in the GGP superconducting gravity data. J Geodyn, 2004, 38: 307–324
14 Xu J Q, Sun H P, Ducarme B. A global experimental model for gravity tides of the Earth. J Geodyn, 2004, 38: 291–304
15 Xu H Z, et al. Geodetic Studies on Tibetan Plateau (in Chinese). Wuhan: Hubei Science and Technology Press, 2001. 3–67
16 Mao H Q, Xu H Z, Song X L, et al. East-west gravity tidal profile of China (in Chinese). Chin J Geophys, 1989, 32: 62–69
17 Hinderer J, Crossley D. Scientific achievements from the first phase (1997–2003) of the Global Geodynamics Project using a worldwide network of superconducting gravimeters. J Geodyn, 2004, 38: 237–262
18 Zerbini S, Richter B, Negusini M, et al. Height and gravity variations by continuous GPS, gravity and environmental parameter observations in the southern Po Plain, near Bologna, Italy. Earth Planet Sci Lett, 2001, 192: 267–279
19 Richter B, Zerbini S, Matonti F, et al. Long-term crustal deformation monitored by gravity and space techniques at Medicina, Italy and Wettzell, Germany. J Geodyn, 2004, 38: 281–292
20 Xu J Q, Zhou J C, Luo S C, et al. Study on characteristics of long-term gravity changrs at Wuhan station. Chin Sci Bull, 2008, 53: 2033–2040
21 Sun H P, Xu J Q, Li Q. Detail spectral structure of Earth's gravity field and its application (in Chinese). Prog Geophys, 2006, 21: 345–352
22 Xu H Z, Sun H P, Xu J Q, et al. International tidal gravity reference values at Wuhan station. Sci China Ser D-Earth Sci, 2000, 43: 77–83
23 Vauterin P. Tsoft: Graphical & interactive software for the analysis of Earth tide data. In: Ducarme B, Paquet P, eds. Proceedings of the 13th International Symposium on the Earth Tides, Brussels, 1998. 481–486
24 Wenzel H G. The nanogal software: data processing package ETERNA 3.3. Bull Inf Marées Terrestres, 1996, 124: 9425–9439
25 Farrell W E. Deformation of the Earth by surface loads. Rev Geophys Space Phys, 1972, 10: 761–797
26 Xu H Z, Mao W J. Correction models for ocean loading tides in Chinese continent (in Chinese). Sci China Ser B, 1988, 9: 984–994
27 Agnew D. A program for computing ocean-tide loading. J Geophys Res, 1997, 102: 5109–5110
28 Schwiderski E W. Ocean Tides I, Global ocean tidal equations. Marine Geod, 1980, 3: 161–217
29 Egbert G, Bennett A, Foreman M. TOPEX/Poseidon tides estimated using a global inverse model. J Geophys Res, 1994, 99: 24821–24852
30 Le Provost C, Genco M, Lyard F, et al. Spectroscopy of the ocean tides from a finite element hydrodynamic model. J Geophys Res, 1994, 99: 24777–24797
31 Andersen O B. Global ocean tides from ERS-1 and TOPEX/POSEIDON altimetry. J Geophys Res, 1995, 100: 25259–25429
32 Matsumoto K, Takanezawa T, Ooe M. Ocean tide models developed by assimilating TOPEX/POSEIDON altimeter data into hydrodynamical model: A global model and a regional model around Japan. J Oceanogr, 2000, 56: 567–581

33 Lefèvre F, Lyard F, Le Provost C, et al. FES99: A global tide finite element solution assimilating tide gauge and altimetric information. J Atmos Ocean Technol, 2002, 19: 1345–1356
34 Zhou J C, Xu J Q, Sun H P. Accurate correction models for tidal gravity in Chinese continent (in Chinese). Chin J Geophys, 2009, 52: 1474–1482
35 Merriam J B. Atmospheric pressure and gravity. Geophys J Int, 1992, 109: 488–500
36 Sun H P. Atmospheric gravity Green's function. Chin Sci Bull, 1997, 42: 1712–1719
37 Boy J P, Gegout P, Hinderer J. Reduction of surface gravity data from global atmospheric pressure loading. Geophys J Int, 2002, 149, 534–545
38 Luo S C, Sun H P, Xu J Q. Theoretical computation of the barometric pressure effects on deformation, gravity and tilt (in Chinese). Chin J Geophys, 2005, 48: 1288–1294
39 Kroner C, Jentzsch G. Comparison of different barometric pressure reductions for gravity data and resulting consequences. Phys Earth Planet Inter, 1999, 115: 205–2187
40 Xu J Q, Sun H P, Zhou J C. Experimental detection of the inner core translational triplet. Chin Sci Bull, 2010, 55: 276–283
41 Xu J Q, Sun H P, Luo S C. Study of the Earth's free core nutation by tidal gravity data recorded with international superconducting gravimeters. Sci China Ser D-Earth Sci, 2002, 45: 337–347